PCCP

Accepted Manuscript

ROYAL SOCIETY OF CHEMISTRY

www.rsc.org/pccp

Journal Name

RSCPublishing

ARTICLE

Electrolyte Ion Adsorption and Charge Blocking Effect at the Hematite/Aqueous Solution Interface: An Electrochemical Impedance Study using Multivariate Data Analysis

Cite this: DOI: 10.1039/x0xx00000x

Received ooth January 2012,
Accepted ooth January 2012

DOI: 10.1039/x0xx00000x

www.rsc.org/

K. Shimizu[a*], J. Nyström[b], P.Geladi[b], B. Lindholm-Sethson[a], and J.-F. Boily[a]

A model-free multivariate analysis using singular value decomposition is employed to refine an equivalent electrical circuit model in order to probe the electrochemical properties of the hematite/water interface in dilute NaCl and NH_4Cl solutions using electrochemical impedance spectroscopy. The result shows that the surface protonation is directly related to the mobility and trapping of charge carriers at the mineral surface. Moreover, the point of zero charge can be found on the pH where the charge transfer resistance is highest, in addition to the minimum double layer capacitance. Inner-sphere interaction of the NH_4^+ ion with the surface is indicated by an increase of capacitance for charge carrier trapping from the protonated surface as well as lower double layer capacitance and open circuit potential. It is clear that the intrinsic electrochemical activity of hematite depends on the degree of surface (de)protonation and other inner-sphere adsorption, as these processes affect the charge carrier density in the surface state. This work also highlights an important synergistic effect of the two spectral analyses that enables EIS to be utilized in an in-depth investigation of mineral/water interfaces.

1. Introduction

Hematite is naturally abundant and one of the most stable iron minerals in Earth's upper crust. It plays an important role as an electrocatalyst in renewable energy researches[1-3] as well as in various biogeochemical processes in the natural environment, such as transportation of pollutants in groundwater[4] and atmosphere[5,6] and microbial metabolisms. Understanding the chemistry of the hematite/water interface in common electrolytic solutions is therefore key to improve its catalytic activity and to uncover the mechanisms of various geochemical processes.

All metal oxide/water interfaces are strongly influenced by electric potentials generated from adsorbed potential-determining ions (p.d.i.). The charge-storage capability of these interfaces is generally described in terms of a molecular capacitor whereby p.d.i. and electrolyte counter ions are separated by a charge-free layer of water molecules. Although this basic concept has been packaged through classical electrical double layer models, recent findings are now calling for an improved description of interfacial models.[7-10] As an intrinsic part of interfacial models, experimentally derived electrical double layer properties such as electric potentials are needed and must be interpreted in the context of these findings. These values should be particularly beneficial in accounting for electrostatic contributions to free energies of reactions taking place across metal oxide/water interfaces. In order to conduct surface potential measurement, a mineral must be found or made with adequate electrical conductivity. For this reason and because of its environmental and technological importance, hematite (α-Fe_2O_3) is employed in the present study. Open circuit potential (E_{oc}) measurements of hematite electrodes exposed to aqueous solutions typically display sub-Nernstian behavior with respect to pH and, when corrected for the electrochemical cell constant, are often equated to p.d.i.-derived surface potentials.[11-13]

A single mineral electrode used for E_{oc} measurements offers even greater possibilities when studied by electrochemical impedance spectroscopy (EIS). It can probe multiple processes with different time constants in a single experiment by retrieving various capacitive and resistive properties of the interface. This non-discriminatory and sensitive approach is highly useful for investigations of fundamental reaction kinetics and mechanisms and has been applied in various, often complex, physico- and bioelectrochemical systems.[14-17] An impedance spectrum is obtained from measurement of changes in the voltage-to-current ratio while the fixed amplitude AC voltage is superimposed on the constant bias voltage. The impedance is the ratio of the Fourier transforms of the applied voltage and measured current and is represented as a complex number. The result is often presented in a complex plane plot, which is a plot of real against imaginary impedance, or a bode

plot, which shows magnitudes and phase shifts as a function of frequency.[18] Interfacial processes can be graphically elucidated from these plots[19] although an equivalent electrical circuit model is typically employed. In the model approach, frequency-resolved interfacial processes are expressed using electrical circuit elements (e.g., resistors and capacitors). Alignments of elements (parallel and serial connections) should represent the physical reality of an interface of interest (hence it is an *equivalent* electrical circuit model). This can be derived mathematically[20,21] and/or developed experimentally[2,22-24].

Previously, EIS was used to show that hematite/water interface has systematic dependence of interfacial capacitance and charge diffusion rate on pH.[25] Furthermore, specific adsorption of ammonium ion is assumed to have suppressed surface protonation and blocked charge development causing interfacial capacitance to be lower in NH_4Cl solution than in NaCl solution. Such competitive adsorption may play an important role in natural dissolution/weathering of hematite as well as transport and bioavailabity of amino compounds. Hence further investigation has been warranted for physicochemical aspects of inner sphere adsorption.

The equivalent circuit model used in the previous study (Scheme 1) did not fully trace salient features in the low frequency region which response is predominantly inner sphere processes. Consequently, it is concerned that the peculiar interaction of the hematite surface and ammonium specie observed previously by a cryogenic XPS study[26] may not be accurately probed. Modification in the equivalent circuit model is however difficult because of a lack of understanding of the nature of cation-hematite surface interaction. To make matters worse, an equivalent circuit model does not necessarily provide a unique solution, that is, a model could provide a satisfying fit even if it is does not represent the physical reality of an electrode/water interface.[27] These issues regarding modeling strategies have been a concern among researchers[16,28,29] and thus call for a complementary approach.

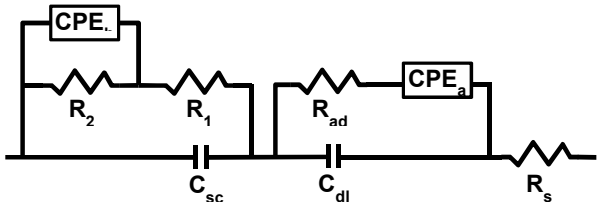

Scheme 1 Equivalent circuit model for hematite/electrolytic solution. Left-hand side includes space charge capacitance, C_{sc}, and charge recombination/trapping capacitance, CPE_h ($=(j\omega)^{-\phi}T_h^{-1}$) and resistance, R_1, and charge transfer resistance, R_2, are of bulk hematite. The solution side of the interfacial process is described by solution resistance, R_s, double layer capacitance, C_{dl}, (de)protonation (or inner-sphere interaction) resistance, R_{ad}, and capacitance, CPE_{ad} ($=(j\omega)^{-\alpha}T_{ad}^{-1}$).

In this work, we utilize singular value decomposition (SVD) to analyze impedance spectra. SVD is a technique related to principal component analysis for decomposing a large multivariate data matrices into a small number of meaningful (systematic) components and noise to ease interpretation.[30,31] Multivariate data analysis for chemical research (i.e., Chemometrics) was established by Kowalski, Massart and Wold in 1970's.[32] However, its application had almost exclusively been for real number datasets. Initial attempt to utilize Chemometric to process impedance spectra is reported by Lindholm-Sethson et al.[33] In their work impedance spectrum was analyzed as two sets real numbers, phase shift and magnitude. Geladi et al.[34] introduced complex number principal component analysis in 2007 enabling SVD to analyze impedance spectra in complex plane. It was used to study effects of various ionic strengths, equilibration times, analyte concentrations, and types of electrolyte ion on polypeptide-electrode interaction using the SVD-EIS integrated approach.[34] Such minor features in raw data are not always perceived in the traditional equivalent circuit modeling approach. Works by Lindholm-Sethson and co-workers[17,34,35] have further demonstrated that SVD is an valuable tool for development of capacitive (bio)sensors that do not depend on electrochemical activity of analyte. Chemometrics was used to analyzed skin impedance collected on various body parts using a specially designed biosensor for determination of sverity of the skin and nerve disorders of diabetic patients as well as for in vivo selective diagnosis of human skin melanoma from other tumors by.[17,35] For the other application, Ulrich et al.[36] carried out quantitative analysis of nitrite and pH by applying partial least square analysis on impedance spectra collected in industrial cutting fluids. These studies clearly show that principal component analysis can be a practical analytical tool for a sample matrix can be too complex to rely on a single equivalent circuit model.

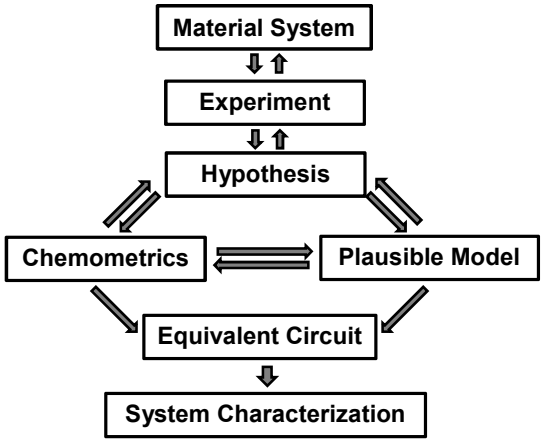

Scheme 2 Box diagram showing approach to an investigation of a system using electrochemical impedance spectroscopy.

SVD alone is not, however, sufficient in physical electrochemistry because it does not generate numerical solutions. In other words, scores of a principal component can only define a trend that spectra deviate with respect to an independent variable. Exact physical process(es) that give(s) rise to it must be found using another technique, i.e., equivalent electrical circuit modelling. In the present work, EIS is carried out on hematite electrode in NaCl and NH_4Cl solutions with various pHs. Impedance spectra are then subjected to the joint analysis as formulated in the flow diagram in Scheme 2. The pH dependences of SVD-derived scores must be present in a plausible model imposed by the initial hypothesis. Failure to emulate score-pH plots by circuit elements is used as an objective criterion to test alternative models. Once pH dependency of circuit elements are matched with that of scores, the plausible model can then be used as an equivalent circuit for system characterization. As will be shown herein, one of the strengths of this approach is its ability to resolve features that

have been overlooked in previous investigations. This paper describes an effect of surface (de)protonation and specific adsorption of electrolyte ion on charge carrier density of hematite surface as well as the mechanistic aspects of NH_4^+-hematite interaction and the subsequent charge blocking effect that hinders surface protonation.

2. Method

General function of SVD is that it projects data points on a two-dimensional window to find a major trend, a unit vector called the principal component.[37] Each principal component consists of scores that depict spectral change derived from alteration of the experimental condition (i.e., pH in this work) and loadings that can be used to elucidate time constants of specific processes.[38] Method described herein is designed for datasets with complex numbers such as impedance spectra developed by Geladi et al.[34], and to some extent it differs from that for real number datasets. Real number principal component analysis has been used for electrochemical analysis as reported by Jimenez-Perez et al.[39], Ross and Venton[40], Casillia et al.[41] There number of literatures available to provide examples of real number SVD.[42-46]

Impedance spectra of all operative conditions under which the data were collected are referred to as objects and are grouped into a two-dimensional matrix. Real and imaginary impedances at all frequencies form individual vectors **r** and **x**, respectively, and total impedance is therefore expressed as a complex vector ($j^2 = -1$):

$$\mathbf{z} = \mathbf{r} + j\mathbf{x} \quad \text{(Eqn. 1)}$$

where **z** is a row vector with *K* elements, which is equivalent to the number of frequencies applied in a single measurement. As experiments are repeated with systematically modified conditions (i.e., pH), the vectors form an $I \times K$ matrix **Z** where *I* is the total number of measurements.

A SVD of this matrix, $\mathbf{Z} = \mathbf{usv}^H$, produces unitary abstract score vectors in matrix **u**, their corresponding lengths in a diagonal singular value s (a real number), and unitary factor loadings in the transposed conjugated matrix $\mathbf{v}^H$.

$$\mathbf{Z} = \mathbf{u}_1 s_1 \mathbf{v}_1^H + \mathbf{u}_2 s_2 \mathbf{v}_2^H + ... + \mathbf{u}_A s_A \mathbf{v}_A^H + \mathbf{E} \quad \text{(Eqn. 2)}$$

where subscripts indicates the principal component and **E** is the residual matrix of size I × K. The advantage of the above decomposition is that the results are in order of s_a, that is, statistically, $s_1 > s_2 > s_3$, and so on. A large singular value indicates that the part of the equation contains significant systematic information while the opposite suggests less systematic and noisier. Orthonormality property makes the interpretation easy because $\mathbf{u}_i$ can be interpreted independent of $\mathbf{u}_j$ and $\mathbf{v}_i$ can be interpreted independent of $\mathbf{v}_j$ The orthonomality properties are:

$\mathbf{u}_i^H.\mathbf{u}_j = 0$ if i is not equal to j;

$\mathbf{u}_i^H.\mathbf{u}_j = 1$ if i is equal to j;

$\mathbf{v}_i^H.\mathbf{v}_j = 0$ if i is not equal to j; and

$\mathbf{v}_i^H.\mathbf{v}_j = 1$ if i is equal to j.

Period (.) in the above equation is the vector multiplication symbol (scalar product). The vectors are called unitary instead of orthonormal for real number SVD. A difference for interpretation is simply that each vector $\mathbf{u}_a$ or $\mathbf{v}_a$ can be shown as a Wessel plot (complex plane plot). An appropriate number of principal components is determined based on the relative size of the sum of squares of the singular value (SS_i):

$$100\% = SS_1 + SS_2 + \ldots + SS_a + SS_E \quad \text{(Eqn. 3)}$$

We set the SS value below 0.5% to be treated as the residual, extractable errors, SS_E, which might arise from sources such as instrument noise.

SVD-derived scores were compared with physical parameters extracted from an equivalent circuit model and the goodness of fit was determined with a χ^2 test ($p<0.05$). SVD calculations were carried out with Matlab (The Mathworks, Inc.).

3. Experimental

3.1 Chemicals and Materials

Ammonium chloride (ACS/ISO grade) was obtained from Merck (pro analysi). Hydrochloric acid and sodium chloride were from VWR (analar normapur, Leuven, Belgium). Pellets of sodium hydroxide were purchased from Eka Chemical AB (pro analysi, Bohus, Sweden) and aqueous ammonia was obtained from Scharlau Chemie (25%, reagent grade, Sentmenat). Standard titrants of acid and base were prepared using house-distilled deionized water filtered through a Milli-Q plus 185 QPAK purification pack (lot #F9MN39572). Nitrogen gas (99.99%) was further purified to remove CO_2 by passing through traps of 0.1 M NaOH and Milli-Q water. Solution pH was measured with a glass electrode (Orion 8103SC), which was calibrated daily using pH buffers (pH 3, 4, 7, and 9). A Ag/AgCl (3M NaCl) reference electrode was purchased from BASi (West Lafayette, USA) and a Pt mesh auxiliary electrode was constructed in-house.

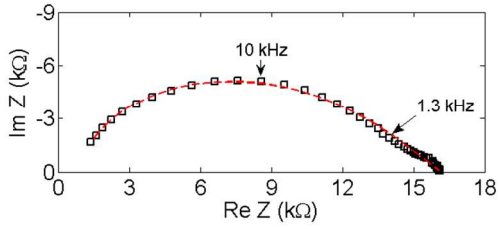

Fig. 1 Electrochemical impedance spectra of hematite crystal collected at 0 bias voltage and 25 mV amplitude and frequency ranged from 100 kHz to 1 Hz. Fit result is shown by a red dash-line.

The hematite (4.99 mm × 4.44 mm × 2.05 mm) used in this study was a natural specimen obtained from an unspecified location (SurfaceNet, Rheine, Germany). It was originally cut and chemically and mechanically polished along the (001) plane but was damaged after annealing at 1000 °C for 17 h in air. It was thereafter re-polished by hand to a mirror finish although the surface sustained visible pits and scratches. An XPS analysis exhibited a characteristic Fe 2p spectra and a binding energy gap between the main O 1s and Fe $2p_{3/2}$ lines for hematite. Moreover, the following impurities were found at the surface: 1.12% F, 1.90% Cr, 0.07% Ag, 0.18% Ca, 1.64% Mo, 2.28% Si, and 0.01% Pb. This specimen was subjected to an EIS analysis prior to electrode preparation by fixing Cu wires on both ends with Ag epoxy and preventing the conductive epoxy from touching the sides. From the resulting

impedance spectra (Fig. 1) the left-hand side of the equivalent circuit model in Scheme 1 was constructed. Resistance of the mineral taken from the sum of all resistance values in the equivalent circuit model was 14.1 kΩ.

3.2 Electrochemical impedance spectroscopy

For construction of a working electrode, hematite was fixed in a Tygon tube with epoxy resin, and electrical connection was established by attaching a Cu wire with Ag epoxy. The exposed surface of the hematite electrode was hand-polished with an aqueous slurry of 5 µm alumina and sonicated briefly in Milli-Q water to remove alumina residue. Electrochemical measurements were carried out in 0.1 M NaCl or NH_4Cl under N_2 atmosphere with pH varying between 3.8 and 11.9 (3.5 to 10.6 for the NH_4Cl system). Equilibration time was at least 40 min or until the drift of E_{oc} was less than 0.3 mV/min. Solution was stirred with a stirring magnet during E_{oc} measurement. EIS was conducted in a three-electrode cell configuration using a Princeton Applied Research 273A potentiostat/galvanostat with a model 1250A frequency response analyzer (Solartron Analytical). Zeplot® (V. 3.10 Scribner Associates inc.) was the operating software for impedance analysis and Corrware® was used to monitor E_{oc}. Bias voltages were taken from E_{oc} and frequency was varied from 100 kHz to 0.1 Hz with amplitude of 25 mV in order to compensate for low current output. The impendence data were validated against Kramers-Kronig transform[47,48], and then fitted with an equivalent electric circuit model using Zview® (v. 3.1). The optimized numerical values of elements are provided in Table 1 at the end of this article.

4. Results and Discussion

4.1 The NaCl system

In a dilute NaCl solution, the hematite/aqueous solution interface chemistry undergoes adsorption of p.d.i., namely H^+ and OH^-, and the electrolyte ion, a prerequisite to the formation of an electrical double layer.[8,49-51] This well-studied system is appropriate for testing the applicability of SVD to attest that findings from an equivalent circuit model represent genuine interfacial processes. Fig. 2a exhibits the characteristic impedance spectrum of a hematite electrode in 0.1 M NaCl along with a fit generated by the equivalent circuit model in Scheme 1. For all spectra, the fit generates low χ^2 values of between 10^{-4} and 10^{-5}. A distorted semi-circle in the high frequency region (Fig. 2a inset) is originated by the electrode itself (as depicted in Fig. 1) , which can be fitted using the left-hand side of the equivalent circuit model in Scheme 1. Low frequency impedance indicates charging at the aqueous side of the interface and is modeled with double layer charging in parallel with p.d.i adsorption resistance and capacitance (the right-hand side of Scheme 1). A constant phase element (CPE_{ad}, $Z_{CPE} = (j\omega)^{-\alpha} T_{ad}^{-1}$) is applied for adsorption capacitance in order to justify the less than ideal capacitive behavior of the electrode surface owing to variation in reaction time constant, energy, and surface morphology.[52-54] This is suitable for adsorption of p.d.i because surface condition or morphology should affect the dispersion of reaction time constant of inner-sphere interaction more than that of the double layer charging.[55] A CPE was also applied for double layer capacitance; however, it generated considerably worse fit result.

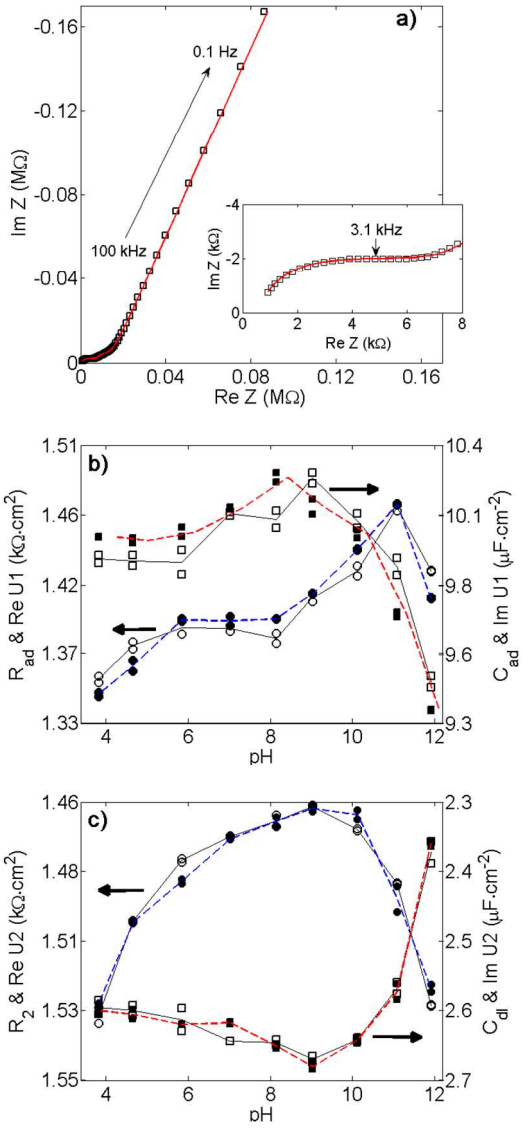

Fig. 2 (a) Characteristic impedance spectra of hematite electrode in 0.1 M NaCl . Fit result generated from the equivalent circuit model in Scheme 1 is shown by red dash-line. Inset: impedance spectra at high frequency region exposing a semi-circular response of hematite crystal. (b) Real (○) and imaginary (□) scores from the first principal component and R_{ad} (■) and C_{ad} (●) as a function of pH. (c) Real (○) and imaginary (□) scores from the second principal component and R_2 (■) and C_{dl} (●) as a function of pH.

Fig. 2b shows that scores from the first principal component are in excellent agreement with the scattering patterns of adsorption resistance (R_{ad}) and capacitance (C_{ad}, calculated according to Brug et al.[56] as $C_{ad} = T_{ad}^{(1/\alpha)} \cdot R_{ad}^{((1-\alpha)/\alpha)}$). It provides the first independent verification for incorporating a surface protonation model in the circuit model and suggests its concomitant development with the electrical double layer. This component expresses the foremost significant changes in the impedance spectra, with 92.3% of the total spectra variation is explained, indicating that surface (de)protonation of hematite surface (hydr)oxo groups is the predominant interfacial process in this solution. This is an important finding because theories for mineral/water interfaces have been based on surface charge development probed using potentiometric acid-base titration.[57]

The relaxation time constant ($\tau^{-1}= (C_{ad}\cdot R_{ad})^{-1}$) for surface (de)protonation obtained from the aforementioned C_{ad} and R_{ad} values is 71 Hz. The relaxation time derived from this (14 ms) is in good agreement with the lifetime of hydroxyl protons on aluminum-hydroxide polyoxocation measured using ^{1}H NMR.[58] The time constant is however significantly shorter than the hematite (001) crystal plane, which varied proportionally from 4.2 s to 0.7 s with respect to pH.[56] This may be due to the synergy of the three surface functional groups that promotes specific bindings or ion/surface hydroxo group exchange.[57,59,60] In such cases, a constant phase element is appropriate for surface (de)protonation capacitance.

The second principal component describes 6.9 % of data, and the real and imaginary scores are in agreement with R_2 and C_{dl}, respectively (Fig. 2c). The point of zero charge (PZC) of the electrode can be assumed to be around pH 9, where double layer capacitance is minimal. R_2 is part of the equivalent circuit model that describes the internal properties of the hematite electrode. Its dependence on the solution pH indicates that it describes a charge transfer process to the solution, as previously noted by Klahr et al.[61] Then, CPE_h and R_1 are the pseudo-capacitance and resistance for surface state charge trapping. Since no faradaic process takes place in the present study, R_2 describes the resistance that the hematite surface feels when surface (de)protonation and any other specific (inner-sphere) adsorption of charged ions take place. Furthermore, PZC appears where the resistance value is highest, which suggests that the surface is less likely to accept or release p.d.i. Decreases in resistance in both acidic and basic pHs are attributable to an increase in surface (de)protonation.

It is worth mentioning that there were discrepancies between the model-extracted capacitance and the imaginary scores after the initial evaluation. We observed that C_{dl} decreased more rapidly than the score in acidic pHs and increased more slowly in basic pHs. This could not be corrected by modifying the composition of Scheme 1. Instead, it was solved by slightly varying the ϕ value in CPE_h, which was otherwise fixed at 0.5. It was lowered for acidic pHs (0.487 at pH 3.8 and 0.496 for pH 4.7) and raised for basic pHs (0.505 for pH 11.1, and 0.52 for pH 11.9). The pH dependences of previously discussed circuit elements are not affected by this operation; however it affected CPE_h as well as R_1, neither of which showed pH dependence during the initial fitting. The pseudo-capacitance, T_h, is high at acidic pH and low at basic pH and trapping resistance, R_1, shows the opposite behavior (Table 1). This implies that increasing positive charge at the surface prompts electron trapping in acidic solution, increasing the chance of charge recombination, whereas the negatively charged surface repels electrons from the interface. This interpretation is consistent with some of the known properties of this mineral such as that electrocatalysis of water oxidation[61], which requires hole transfer, is generally carried out at pH 13 and that the rate of reductive dissolution, which requires high electron density at the surface, is faster at lower pH[62]. Hence it has shown that the model results can be made more physically realizable by allowing SVD analysis to impose restrictions on circuit elements.

4.2 The NH_4Cl system

Interaction of NH_4^+ with hematite is more intricate because of the specific interaction with surface (hydr)oxo functional groups (e.g., $\equiv$Fe-$OH^{-1/2}\cdots HNH_3^+$).[26] This process notably shifts the pKa of the NH_4^+/NH_3 pair from 9.3 in bulk aqueous solution to 8.4 at the hematite/water interface. Moreover, it is suspected to have induced a charge-blocking phenomenon[26] although this remains to be elucidated from the EIS data.

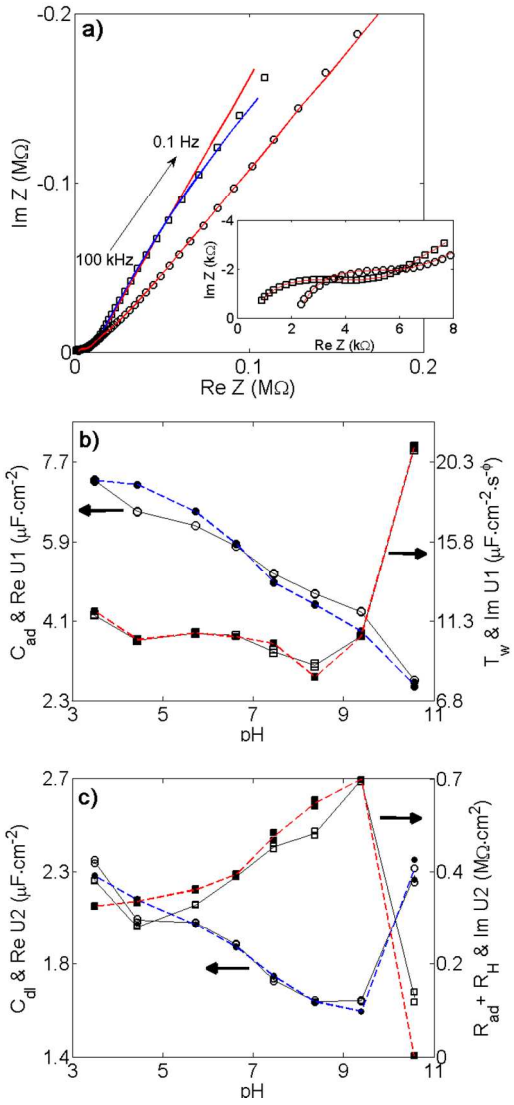

Fig. 3 (a) Characteristic impedance spectra of hematite electrode in 0.1 M NH_4Cl at (□) pH 5.72 and (○) pH 10.56. Fit result generated from the equivalent circuit model of Scheme 1 is shown by a red line and that of Scheme 3 by a blue line. Inset: impedance spectra at high frequency region exposing a semi-circular response of hematite crystal as well as a horizontal offset attributed to lower dielectric of aqueous ammonia than water. (b) Real (○) and imaginary (□) scores from the first principal component and C_{ad} (■) and T_h (●) as a function of pH. (b) Real (○) and imaginary (□) scores from the second principal component and R_{ad} + R_H (■) and C_{dl} (●) as a function of pH.

Characteristic impedance spectra and fits generated from the model in Scheme 1 are shown in Fig. 3a. The impedance spectrum at pH 10.6 is quite different from the rest, with particularly higher solution resistance (spectrum is shifted horizontally to higher Re Z, as shown in Fig. 3a inset). This may be because, at that pH, ammonia is a dominant species and lowers dielectric constant of the solution. The impedance spectrum at the basic pH also deviates from the rest in the low

frequency region, which may indicate the lack of the specific interaction mentioned above.

We first examined whether the solution resistance has significant impact on overall interfacial process by conducting SVD analysis separately for untreated spectra and R_s subtracted spectra, but no significant difference in the results was observed. Second, we tested whether the impedance spectra from pH 10.56 could obscure the chemometrical analysis. To check this, analysis was carried out by excluding impedance spectra collected at pH 10.56. When the result was compared with the unmodified dataset, the first principal component was fairly similar but the second component differed considerably. Because the first components reasonably agree in two datasets, impedance spectra from the basic pH were not considered as an outlier. Nevertheless, the discrepancy in the second components suggests that there is an interfacial process that is uncommon between the basic pH and all the other pHs. In fact, the initial fitting results of Scheme 1 did not match with all the components extracted from the SVD analysis. Therefore it was necessary to modify the equivalent circuit model initially applied.

We speculated that, if the specific adsorption of ammonium ion limits the surface protonation and subsequent electrostatic adsorption of electrolyte ions, then there must be significant resistance against free protons to reach the electrode surface. This is analogous to the corrosion of polymer-coated metals, and an additional interfacial process can be accorded in the equivalent circuit model with a resistance element, R_H, in parallel with the adsorption pseudo-capacitance, as displayed in Scheme 3. This new model provides a good curve fitting (Fig. 3a, blue line) with the same level of χ^2 values for all solutions except for pH 10.56, at which it failed to generate an acceptable fit. This suggests that the NH_3-surface specific interaction does not occur at the basic pH. The results obtained from the new equivalent circuit model are compared with the SVD analysis.

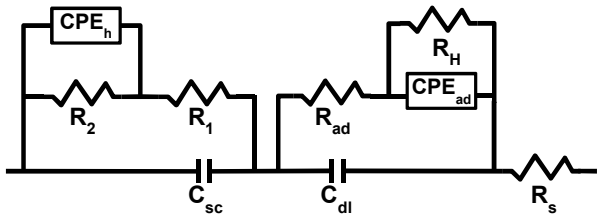

Scheme 3 Modified equivalent circuit model for hematite/ electrolytic solution interface. R_H indicates the proton transfer resistance, or the charge blocking effect, by surface adsorbed ammonium ion. The rest of the circuit elements are as described in Scheme 1 as well as in the text.

The first principal component for this system accounts for 99.1 % of the variance of the EIS data collected for this system. In comparison with the previous NaCl system (i.e., 92.3% explained by the first component), the interfacial process explained here is substantially more dominant than protonation alone. Fig. 3b illustrates that the real score has the closest pH dependence on C_{ad}. The smaller specific adsorption capacitance in NH_4Cl than in NaCl, as shown in Table 1, may indicate that the inner-sphere adsorption of NH_4^+ occupies multiple binding sites. Further investigation is needed to discuss the exact binding mechanism. Still, a decrease in capacitance caused by specific adsorption of electrolyte ions can be explained in terms of the variable capacitance model[63]. According to the model, the specific adsorption of an electrolyte ion extends surface structures. This causes the compact plane to extend out further than that of the protonated surface and lowers potential and double layer capacitance, as in E_{oc} and C_{dl} (Table 1). The imaginary score, which illustrates the behavior of T_h, shows rather marginal change in pH below 8.4 and a sharp increase towards the alkaline condition (Fig. 3b). This pseudo-capacitance, which describes surface state charge trapping, is roughly twice as much as that in the NaCl system (Table 1), contrasting with adsorption capacitance on the solution side, which is higher in the NaCl system. Since R_2 is also lower in NH_4Cl than in NaCl, it is evident that the specific adsorption NH_4^+ ion promotes surface states electron trapping. This should cause hematite to be more likely to be reduced in NH_4Cl solution than NaCl solution under a similar condition. Indeed, a hematite electrode did generate higher reduction current in NH_4Cl solution during a cyclic voltammetric study reported by Shimizu et al.[25]

The second component explained 0.9% of the data. The real score-pH plot can be traced with the sum of R_{ad} and R_H, and C_{dl} can be fitted to the imaginary score by adjusting the ϕ value of CPE_h (Fig. 3c). R_{ad} is considerably smaller than R_H (Table 1), and it is practically negligible at most pHs except for pH 10.56, at which R_H is zero. The C_{dl}-pH plot in Fig. 3c shows the same PZC as in the previous system suggesting a comparable charging attribute of the mineral surface in both electrolytic solutions, despite the charge-screening effects of the hydrogen-bonded NH_4^+ species. Milder increment of resistance with pH leading up to pH 9.39 in comparison with a decrease between pH 9.39 and 10.56 suggests that the amount of the surface-bound NH_4^+ is relatively unchanged by pH. This interpretation can be confirmed by the pH-T_h behavior, which also shows only a marginal change in the same low pH range (Fig. 3b). These two elements are physically related because specifically adsorbed ion modifies the surface structure, likely affecting the probability of trapping charges in the surface state. Sudden drop of resistance together with similar changes in T_h and C_{dl} may suggest that the surface is free of the insulating layer at pH 10.56. Despite that, the C_{dl} value in the NH_4Cl system at the basic pH is still slightly lower than that in NaCl (Table 1). This may be because charge-neutral ammonia, which is the dominant species in the solution at pH 10.56, is not attracted to the negatively charged surface as much as the Na^+ ion is. The current study reveals the intrinsic property of hematite whereby charge carriers are mobilized with the surface (de)protonation determining electrochemical activity of the mineral. Further investigation is currently planned for interactions of oxocarbon anions with the hematite surface.

5. Conclusions

Electrolyte ion adsorption mechanisms of a hematite electrode in dilute monovalent electrolytic solution are probed by means of electrochemical impedance spectroscopy. A spectral analysis using an equivalent circuit model is systematically improved by using a model-free SVD that extracts pH dependence of interfacial processes that have significant impact on impedance spectra. The results show that, in a dilute NaCl solution, surface protonation is a predominant interfacial process. It is found that the relaxation time of the inner-sphere interaction (14 ms) is shortened from (001) crystallographically oriented surface. This is attributed to the fact that the three surface functional groups, which are probably present on the hand-polished electrode, promoted specific binding or ion/surface hydroxo group exchange. SVD suggests

Table 1. Fit result of the equivalent circuit model for the hematite electrode*

NaCl

pH	E_{oc} (V)	χ^2 (10^{-4})	R_s ($\Omega\cdot cm^2$)	C_{dl} ($\mu F\cdot cm^{-2}$)	T_{ad} ($\mu F\cdot cm^{-2}\cdot s^{-\varphi}$)	α	R_{ad} ($k\Omega\cdot cm^2$)	C_{sc} ($nF\cdot cm^{-2}$)	R_1 ($\Omega\cdot cm^2$)	R_2 ($k\Omega\cdot cm^2$)	T_h ($\mu F\cdot cm^{-2}\cdot s^{-\varphi}$)	ϕ
3.82	0.212	0.76	158 (1)	2.40 (0.03)	33.2 (0.1)	0.722	1.35 (0.01)	8.12 (0.08)	437 (9)	6.71 (0.01)	8.08 (0.20)	0.487
4.66	0.182	0.62	157 (1)	2.38 (0.03)	32.9 (0.1)	0.723	1.36 (0.01)	8.14 (0.07)	457 (7)	6.83 (0.01)	7.73 (0.15)	0.496
5.85	0.148	0.65	157 (1)	2.37 (0.02)	32.8 (0.1)	0.723	1.39 (0.01)	8.17 (0.07)	465 (7)	6.88 (0.01)	7.58 (0.14)	0.500
7.03	0.122	0.63	157 (1)	2.37 (0.02)	32.7 (0.1)	0.725	1.39 (0.01)	8.19 (0.07)	466 (7)	6.95 (0.01)	7.64 (0.14)	0.500
8.14	0.099	0.63	157 (1)	2.34 (0.02)	32.9 (0.1)	0.726	1.40 (0.01)	8.19 (0.07)	463 (7)	6.97 (0.01)	7.59 (0.14)	0.500
9.03	0.084	0.66	158 (1)	2.32 (0.02)	32.5 (0.1)	0.726	1.41 (0.01)	8.21 (0.07)	467 (7)	6.99 (0.01)	7.68 (0.14)	0.500
10.12	0.054	0.70	158 (1)	2.35 (0.02)	32.4 (0.1)	0.724	1.44 (0.01)	8.21 (0.07)	467 (7)	6.98 (0.01)	7.65 (0.15)	0.500
11.09	0.025	1.00	159 (2)	2.43 (0.03)	31.7 (0.1)	0.722	1.47 (0.01)	8.30 (0.08)	481 (8)	6.88 (0.01)	7.62 (0.17)	0.505
11.91	-0.028	1.01	157 (2)	2.61 (0.03)	32.3 (0.1)	0.714	1.41 (0.01)	8.34 (0.08)	497 (7)	6.74 (0.01)	6.94 (0.14)	0.520

NH_4Cl

pH	E_{oc} (V)	χ^2 (10^{-4})	R_s ($\Omega\cdot cm^2$)	C_{dl} ($\mu F\cdot cm^{-2}$)	T_{ad} ($\mu F\cdot cm^{-2}\cdot s^{-\varphi}$)	α	R_H ($k\Omega\cdot$cm2)	R_{ad} ($k\Omega\cdot cm^2$)	C_{sc} ($nF\cdot cm^{-2}$)	R_1 ($\Omega\cdot cm^2$)	R_2 ($k\Omega\cdot cm^2$)	T_h ($\mu F\cdot cm^{-2}\cdot s^{-\varphi}$)	ϕ
3.49	0.146	0.75	153 (1)	2.23 (0.05)	31.9 (0.1)	0.696	360 (11)	1.05 (0.01)	8.38 (0.08)	424 (7)	5.28 (0.06)	11.8 (0.3)	0.480
4.44	0.118	0.69	154 (1)	2.12 (0.05)	29.9 (0.1)	0.702	367 (11)	1.16 (0.01)	8.48 (0.07)	449 (6)	5.17 (0.05)	10.2 (0.3)	0.500
5.72	0.096	0.68	154 (1)	2.00 (0.04)	29.2 (0.1)	0.693	401 (12)	1.17(0.01)	8.49 (0.07)	452 (6)	5.20 (0.06)	10.6 (0.3)	0.500
6.63	0.086	0.67	154 (1)	1.89 (0.04)	28.1 (0.1)	0.685	437 (14)	1.16 (0.01)	8.46 (0.07)	451 (6)	5.15 (0.06)	10.4 (0.3)	0.500
7.46	0.074	0.74	153 (1)	1.75 (0.04)	26.4 (0.1)	0.677	517 (19)	1.13 (0.01)	8.39 (0.08)	449 (7)	5.06 (0.06)	10.0 (0.3)	0.500
8.37	0.059	0.83	154 (1)	1.62 (0.04)	25.1 (0.1)	0.672	599 (26)	1.15 (0.01)	8.43 (008)	467 (7)	4.77 (0.06)	8.1 (0.3)	0.520
9.39	0.024	0.78	164 (1)	1.58 (0.04)	24.2 (0.1)	0.656	665 (30)	1.23 (0.02)	8.44 (0.09)	449 (8)	5.38 (0.07)	10.4 (0.3)	0.490
10.56	-0.008	2.28	520. (3)	2.32 (0.17)	20.8 (0.1)	0.579		2.84 (0.11)	10.2 (0.15)	623 (11)	16.1 (1.5)	21.1 (0.7)	0.460

*Values are corrected for the geometrical surface area of the electrode (0.222 cm^2). Confidence limits shown in parenthesis are given after multiplication by the results of the Student t test.

that charge transfer resistance of the mineral surface is the highest at pH 9.03 in the NaCl system, proposing the PZC of this electrode. This resistance shows a gradual decrease towards both acidic and basic pH, indicating that the hematite surface is more likely to accept charges (i.e., p.d.i.) from the solution. It is concluded from the pH-T_h and pH-R_1 behaviors that acidic pH promotes electron trapping and increases the change of recombination, leading to reductive dissolution. On the other hand, electrons are repelled by the negatively charged surface in basic pH that is prerequisite for hematite to perform electrocatalysis. It is thereby shown that electrochemical activity as well as the PZC of hematite depends on the mobility of charge carriers in the surface state. Formation of an insulating layer in pH below 9.39 is inevitable in the NH_4Cl system, as SVD analysis necessitated the addition of a resister to equivalent electrical circuit model in parallel with adsorption capacitance. It is concluded further to say that specific adsorption of NH_4^+ ion modifies the surface structure and extends the compact layer further out than the protonated surface, resulting in lower C_{dl} and E_{oc} than that in the NaCl system. It is demonstrated that multivariate data analysis for spectral interpretation successfully uncovers an important relation between protonation and charge carrier mobility at the surface that explains the intrinsic electrochemical properties of hematite. This was not possible with an equivalent circuit model alone.

Acknowledgements

This work was supported by the Swedish Research Council (2009-34104-69231-39) and Carl Tryggers, Wallenberg and Kempe Foundations.

Notes and references

[a] Department of Chemistry, Umeå University, 90187, Umeå, Sweden. Email: kenichi.shimizu@chem.ox.ac.uk

[b] Department of Forest Biomaterials and Technology, Swedish University of Agricultural Science, 90183, Umeå, Sweden

1 M.-Y. Li, Y. Wang, C.-L. Liu, H. Gao, Dong, W.-S. *Eletrochimica Acta* 2012, **67**, 187.
2 T. Lopes, L. Andrade, F. Le Formal, M. Gratzel, K. Sivula, A. Mendes, *Phys. Chem. Chem. Phys.* 2014, **16**, 16515.
3 S. Licht, B. Cui, B. Wang, F. F. Li, J. Lau, S. Lin, *Science* 2014, **345**, 637.
4 A. Teutli-Sequeira, M. Solache-Ríos, P. Balderas-Hernández, *Water Air Soil Poll.* 2012, **223**, 319.
5 S. Gómez-Quero, F. Cárdenas-Lizana, M. A. Keane, *J. Catal.* 2013, **303**, 41.
6 C. E. Nanayakkara, P. M. Jayaweera, G. Rubasinghege, J. Baltrusaitis, V. H. Grassian, *J. Phys. Chem. A* 2014, **118**, 158.
7 J. G. Catalano, *Geochim. Cosmochim. Acta* 2011, **75**, 2062.

8 K. Shimizu, A. Shchukarev, Ph. A. Kozin, J.-F. Boily, *Surf. Sci.* 2012, **606**, 1005.
9 K. S. Tanwar, S. C. Petitto, S. K. Ghose, P. J. Eng, T. P. Trainor, *Geochim. Cosmochim. Acta* 2009, **73**, 4346.
10 C. Tournassat, Y. Chapron, P. Leroy, M. Bizi, F. Boulahya, *J. Colloid Interface Sci.* 2009, **339**, 533.
11 P. Zarzycki, S. Chatman, T. Preočanin, K.M. Rosso, Electrostatic Potential of Specific Mineral Surface. *Langmuir* 2011, **27**, 7986.
12 S. Chatman, P. Zarzycki, T. Preočanin, K.M. Rosso, *J. Colloid Interface Sci.* 2013, **391**, 125.
13 J. Lützenkirchen, T. Preočanin, F. Stipić, F. Heberling, J. Rosenqvist, N. Kallay, *Geochim. Cosmochim. Acta* 2013, **120**, 479.
14 I. Shitanda, K. Inoue, Y. Hoshi, M. Itagaki, *J. Power Sources* 2014, *247*, 475.
15 B. B. Berkes, A. Maljusch, W. Schuhmann, A. S. Bondarenko, *J. Phys. Chem. C* 2011, **115**, 9122.
16 X. Domibguez-Benetton, S. Sevda, K. Vandbroekhoven, D. Pant, *Chem. Soc. Rev.* 2012, **41**, 7228.
17 I. Bodén, D. Nilson, P. Naredi, B. Lindholm-Sethson, *Med. Biol. Eng. Comput.* 2008, **46**, 985.
18 A. Lasia, In *Modern Aspects of Electrochemistry*; ed. B. E. Conway, J. Bockris, R. E. White, Kluwer Academic/Plenum, New York, 2002, vol. 32, pp143-248.
19 M. E. Orazem, N. Pébère, B. Tribollet, *J. Electrochem. Soc.* 2006, **153**, B129.
20 C. Gabrielli, P. P. Grand, A. Lasia, H. Perrot, *J. Electrochem. Soc.* 2004, **151**, A1925.
21 S. Sunde, I. A. Lervik, L. E. Owe, M. Tsypkin, *J. Electrochem. Soc.* 2009, **156**, B927.
22 G. A. Ragoisha, A. S. Bondarenko, *Electrochim Acta* 2005, **50**, 1553.
23 S. Lehner, M. Ciobanu, K. Savage, D. E. Cliffel, *J. Electrochem. Soc.* 2008, **155**, P61.
24 A. S. Bondarenko, I. E. L. Stephens, H. A. Hansen, F. Perez-Alonso, V. Tripkovic, T. P. Johansson, J. Rossmeisl, J. K. Norskov, I. Chorkendorff, *Langmuir* 2011, **27**, 2058.
25 K. Shimizu, A. Lasia, J.-F. Boily, *Langmuir* 2012, **28**, 7914.
26 K. Shimizu, A. Shchukarev, J.-F. Boily, *J. Phys. Chem. C* 2011, **115**, 6796.
27 D. D. Macdonald, *Electrochim Acta* 2006, **51**, 1376.
28 M. Sluyters-Rehbach, *Pure Appl. Chem.* 1994, *66*, 1831.
29 B. Grysakowski, J. J. Jasielec, B. Wierzba, T. Sokalski, A. Lewenstam, M. Danielewski, *J. Electroanal. Chem.* 2011, **662**, 143.
30 E. A. Jackson, User's Guide to Principal Components, Wiley, New York NY, 1991, ISBN 0-471-62267-2.
31 I. T. Jolliffe, Principal Component Analysis, 2nd ed., Springer, NY, 2002, ISBN 978-0-387-95442-4.
32 P. Geladi, Chemometrics in Specstrscopy. Part 1. Classical Chemometrics. Spectrochimica Acta B, 2003, 58, 767-782.
33 B. Lindholm-Sethson, S. Han, S. Ollmar, I. Nicander, G. Jonsson, F. Lithner, U. Bertheim, P. Geladi, *Chemom. Intell. Lab. Syst.* 1998, *44*, 381
34 P. Geladi, A. Nelson, B. Lindholm-Sethson, *Anal. Chim. Acta* 2007, **595**, 152.
35 I. Bodén, J. Nyström, B. Lundskog, V. Zazo, P. Geladi, B. Lindholm-Sethson, P. Naredi, *Skin Res. Technol.* 2013, **19**, e473-e478
36 C. Ulrich, D. Louthander, P. Mårtensson, A. Kluftinger, M. Gawronski, F. Björefors, *Talanta* 2012, *97*, 468.
37 L. Eriksson, E. Johansson, N. Kettaneh-Wold, J. Trygg, C. Wikström, S. Wold, Multi- and Megavariate Data Analysis Part I Basic Principles and Applications, Umetrics Academy, Umeå, 2nd edn., 2006, pp 21-38.
38 B. Lindholm-Sethson, J. Nyström, M. Malmsten, L. Ringstad, A. Nelson, P. Geladi, *Anal. Bioanal. Chem.* 2010, **398**, 2341.
39 R. Jimenez-Perez, M. Baro, L. Elie, J.G. Rodriguez, *Int. J. Electrochem. Sc.* 2013, **8**, 3279-3289.
40 A.E.Ross, B.J. Venton, *Anal. Chem.* 2014, **86**, 7486-7493.
41 S. Casillia, M. De Luca, C. Apetrei, V. Parra, A. A. Arrieta, L. Valli, J. Z. Jiang, M. L. Rodriguez-Mendez, J. A. De Saja, *Appl. Surf. Sci.* 2005 **246**, 304-312.
42 K. Beebe, R. Pell, M. S. Seasholtz, Chemometrics, A Practical Guide, Wiley, New York, NY, 1998, ISBN 0-471-12451-6.
43 K. Varmuza, P. Filzmoser, Introduction to Multivariate Statistical Analysis in Chemometrics, CRC Press, Boca Raton, FL, 2009, ISBN 978-1-4200-5947-2.
44 E. Malinowski, Factor Analysis in Chemistry 3rd ed, Wiley, New York, NY, 2002, ISBN 0-471-13479-1.
45 R. Brereton, Chemometrics. Data Analysis for the Laboratory and Chemical Plant, Wiley, Chichester, UK, 2003, ISBN0-471-48977-8.
46 R. Henrion, G. Henrion, Multivariate Datenanalyse. Methodik und Anwendung in der Chemie und verwandten Gebieten, Springer, Berlin, Germany, ISBN 3-540-58188-X.
47 B. A. Boukamp, *Solid State Ionics* 2004, **169**, 65.
48 B. A. Boukamp, *J. Electrochem. Soc.* 1995, **142**, 1885.
49 A. Breeuwsma, J. Lyklema, *J. Colloid Interface Sci.* 1973, *43*, 437.
50 P. Zarzycki, S. Chatman, T. Preočanin, K. M. Rosso, *Langmuir* 2011, *13*, 7986.
51 S. Chatman, P. Zarzycki, T. Preočanin, K.M. Rosso, *J. Colloid Interface Sci.* 2013, **391**, 125.
52 K. S. Cole, R. H. Cole, *J. Chem. Phys.* 1941, **9**, 341.
53 V. M.-W. Huang, V. Vivier, M.E. Orazem, N. Pébère, B. Tribollet, *J. Electrochem. Soc.* 2007, **154**, C99.
54 J.-B. Jorcin, M.E. Orazem, N. Pébère, B. Tribollet, *Electrochim. Acta* 2006, **51**, 1473.
55 S. Kerisit, E. S. Ilton, S. C. Parker, *J. Phys. Chem. B* 2006, **110**, 20491.
56 G. J. Brug, A. L. G. van den Eeden, M. Sluyters-Rehbach, J. H. Sluyters, *J. Electroanal. Chem.* 1984, **176**, 275.
57 K. Shimizu, J.-F. Boily, *Langmuir* 2014, ***30***, 9591..
58 J. R. Houston, B. L. Phillips, W. Casy, *Geochim. Cosmochim. Acta* 2006, **70**, 1636.
59 S. Kerisit, *Geochim. Cosmochim. Acta* 2011, ***75***, 2043.
60 J.-F. Boily, R.D. Lins, *J. Phys. Chem. C* 2009, **113**, 16568.
61 B. Klahr, S. Gimenez, F. Fabregat-Santiago, T. Hamann, J. Bisquert, *J. Am. Chem. Soc.* 2012, **134**, 4294.
62 C. Liu, J. M. Zachara, N. S. Foster, J. Strickland, *Environ. Sci. Tech.* 2007, **41**, 7730.
63 J.-F. Boily, *Langmuir* 2014, **30**, 2009.